A&A 518, A36 (2010)
DOI: 10.1051/0004-6361/201014475

Astronomy & Astrophysics

C_2 emission features in the Red Rectangle

A combined observational⋆/laboratory study

N. Wehres[1,2], C. Romanzin[2,⋆⋆], H. Linnartz[2], H. Van Winckel,[3], and A. G. G. M. Tielens[1,4]

[1] Kapteyn Astronomical Institute, University of Groningen, PO Box 800, 9700 AV Groningen, The Netherlands
e-mail: wehres@strw.leidenuniv.nl
[2] Raymond and Beverly Sackler Laboratory for Astrophysics, Leiden Observatory, Leiden University, PO Box 9513, 2300 RA Leiden, The Netherlands
[3] Instituut voor Sterrenkunde, K.U. Leuven, Celestijnenlaan 200B, 3000 Leuven, Belgium
[4] Leiden Observatory, Leiden University, PO Box 9513, 2300 RA Leiden, The Netherlands

Received 22 March 2010 / Accepted 6 May 2010

ABSTRACT

Context. The Red Rectangle proto-planetary nebula (HD 44179) is known for a number of rather narrow emission features superimposed on a broad extended red emission (ERE) covering the 5000–7500 Å regime. The origin of these emission features is unknown.
Aims. The aim of the present work is to search for potential carriers by combining new observational and laboratory data. This also allows to interpret spectral emission features in terms of actual physical conditions like temperature and density constraints and to trace chemical processes in the outflows of the Red Rectangle.
Methods. Observational spectra have been obtained with the EMMI-NTT at offsets of 3″, 6″, 7″, 11″, 16″ and 20″ distance to the central star HD 44179. The spectra are compared to the outcome of a time-gated laser induced fluorescence laboratory study of an expanding acetylene plasma using a special supersonic pin-hole discharge source. With this set-up the hydrocarbon chemistry in the Red Rectangle nebula is simulated under laboratory controlled conditions. The plasma source has the unique feature to generate electronically and vibrationally excited species at low rotational temperatures. The comparison is facilitated by a simple model for fluorescent emission in the nebula.
Results. Two of the astronomically observed narrow emission bands can be assigned as originating from unresolved rovibronic progressions within the $d^3\Pi_g \rightarrow a^3\Pi_u$ Swan system of the C_2 radical. The band appearance corresponds to a rotational temperature between 200 and 1000 K. The emission is driven by absorption in the C_2 Phillips bands followed by intersystem crossing from the singlet to the triplet state and pumping in the Swan bands.
Conclusions. These observations imply an active (photo)chemistry in the ejecta of the Red Rectangle.

Key words. astrochemistry – stars: AGB and post-AGB – stars: winds, outflows – ISM: abundances

1. Introduction

The Red Rectangle bi-conical reflection nebula was first identified by Cohen et al. (1975) and is associated with the post AGB binary star HD 44179 (Van Winckel et al. 1995). The star itself is visually obscured by a nearly edge-on circumbinary disc (Roddier et al. 1995; Waelkens et al. 1996; Osterbart et al. 1997; Bond 1997) and can only be seen in scattered light. The disk leads outflows into the north-west and south-east direction from the star and creates the appearance of an X-shaped structure. This shape as well as the unique emission spectrum of the nebula have attracted special attention in the past. In the infrared regime emission features have been found at 3.3, 6.2, 7.7, 8.6, 11.3, 13.57 and 14.23 μm (Russell et al. 1978; Waters et al. 1998) that are typical for vibrational fundamentals of polycyclic aromatic hydrocarbons (PAHs). The spectrum at longer wavelengths is rich of narrow emission bands that can be assigned to crystalline silicates (Waters et al. 1998). In the optical regime the spectrum is dominated by an extended red emission (ERE), which is a strong and broad emission feature that covers the region between 5000 and 7500 Å (Schmidt et al. 1980). Different origins have been proposed for this ERE such as photo-luminescence processes within silicates or nanoparticles of carbonaceous grains (Duley 1985; Witt & Boroson 1990; Witt et al. 1998; Ledoux et al. 1998, 2001; Van Winckel et al. 2002; Witt & Vijh 2004). Blue luminescence was detected in the Red Rectangle (Vijh et al. 2004, 2005, 2006) and it was suggested that the ERE and the blue luminescence may arise from fluorescence of PAHs with a size of 14–18 C atoms. Superimposed on the ERE, a peculiar set of narrow emission features has been observed for which identifications are lacking (Scarrott et al. 1992; Sarre et al. 1995; Glinski & Anderson 2002; Van Winckel et al. 2002; Sharp et al. 2006). The ERE is widespread in the interstellar medium, but the narrow emission features are very unique for the Red Rectangle (Witt et al. 2008). Studies have shown that such emission features shift to the blue and become narrower with distance from the central star. These characteristics are the telltale sign of (anharmonic) molecular emission in a cooling outflow. The blueshifts bring the peak positions closer to the wavelength positions of some of the well-known Diffuse Interstellar Bands (DIBs) (Scarrott et al. 1992; Sarre et al. 1995;

⋆ Based on observations collected at the European Southern Observatory, Chile. Program ID: 080.C-0814(A).
⋆⋆ Current address: Laboratoire de Physique Moléculaire pour l'Atmosphère et l'Astrophysique, UMR 7092, Université Pierre et Marie Curie/CNRS, 4 place Jussieu, 75252 Paris Cedex 05, France.

Van Winckel et al. 2002), but for an opposing view see Glinski & Anderson (2002). The DIBs are observed as absorption features through diffuse interstellar clouds and are attributed to electronic transitions of molecular transients (see also Linnartz et al. 2010).

Apart from the PAH and ERE emission, the carbon-rich nature of the nebula has been corroborated by additional molecular detections like CH, CN and CH^+ (Hall et al. 1992; Bakker et al. 1996; Hobbs et al. 2004). The carbon nature of the star is also in agreement with the IR emission spectrum and the PAHs in the circumstellar gas (Leger & Puget 1984). Furthermore, the disk around the central star is oxygen-rich with molecules like OH (Reese & Sitko 1996), ^{12}CO and ^{13}CO, gaseous and perhaps solid state CO_2 and silicate dust (Waters et al. 1998). The presence of carbon-rich material in the outer part of the nebula and the oxygen-rich material in the central part of the nebula indicates a spatially separated chemistry (Waters et al. 1998).

In all, the picture that emerges from these observations is that of an accretion disk surrounding the low mass companion. This accretion disk may have been (previously) fed by Roche lobe overflow from the post-AGB object, and part of the accretion disk material is accelerated outwards in a fast jet evident in the broad Hα and CO (UV) emission components (Sitko et al. 2008; Witt et al. 2009). The narrow Hα component has been attributed to a small HII region close to the binary stars, ionized by UV emission from the accretion disk (Jura et al. 1997; Witt et al. 2009). The submillimeter CO emission originates in a slowly expanding ($\simeq$0.8 km s^{-1}) and Keplerian rotating circumbinary disk (Jura et al. 1997; Bujarrabal et al. 2005). The cool and narrow component in the UV lines of CO presumably represents the PDR separating the HII region from the surrounding, circumbinary, molecular disk. The atomic lines of potassium as well as the CH, CH^+, and CN lines may also originate in this PDR zone. All of these components are "seen" because of scattering into the beam and not directly. Indeed, given the polarization results (Reese & Sitko 1996), the emission of these lines further out in the nebula seems to be largely due to scattering of photons from this PDR zone into the line of sight of the observer.

In the present study, we combine observational data at different distances from the central star (i.e. for different physical conditions and at different chemical stages) and high resolution laboratory data. These are recorded in emission through a supersonically expanding plasma. Such plasma expansions have become a standard to generate molecular transients of astrophysical interest and their applications in astronomy have been reviewed recently by Linnartz (2009). The overall aim of this experimental study is to identify possible carriers of the narrow emission features as observed around the Red Rectangle and simultaneously to follow the chemical evolution in the outflows of this proto-planetary nebula. Here we focus on two narrow emission bands attributed to the C_2 molecule (Sarre 2006; Glinski et al. 2009).

The paper is organized as follows. Section 2 describes the new observations and experimental results and combines these results with existing ones. Section 3 describes the model we use in order to determine the abundance of C_2 in the outflows of the Red Rectangle. Section 4 shows the implications and is followed by the conclusions in Sect. 5.

2. Astronomical observations and data reduction

The astronomical spectra were obtained on February 4 and 5, 2008, at the 3.5 m NTT (New Technology Telescope) at ESO, La Silla in Chile, making use of the EMMI, ESO Multi Mode Instrument, in medium dispersion spectroscopy mode. All observations were carried out using long slit spectroscopy. Long slit settings of 1″ by 200″ were chosen. This has the advantage that light is sampled over only a narrow region at a given distance from the central star in the outflow of the nebula. The slit was oriented perpendicular to the polar direction of the nebula at a constant position angle of 105° east from north at the different offsets from the star. The slit spectrum provides the wavelength versus width (spatial information) and is later collapsed into one single point, which is justified by the constant offset angle perpendicular to the nebula's symmetry axis. That way the S/N ratio increases which helps to obtain high quality spectra even in fainter regions of the nebula further away from the central source. The visual magnitude of the central source HD 44179 amounts to about 9 but is obscured by the nebula. For telescope settings further away from the central star the intensity of the flux is decreasing fast and thus integration times have to be varied with distance from the centre. The observation blocks are specified in Table 1 for three different settings using grating 6 in two different wavelength regimes in order to cover the whole ERE at a resolution of $\lambda/\Delta\lambda = 5000$. Grating 6 was used at central wavelengths of 5870 Å and 6500 Å. Spectra were obtained at the central star as well as at 3″ and 7″ distance. The third setting used grating 7 at larger offsets to the central star (16″ and 20″). Here we recorded spectra covering the whole ERE domain in order to keep integration times realistic. As a consequence the resolution decreased to $\lambda/\Delta\lambda = 2600$. The central wavelength position for this setting was at 6200 Å. For each spectral study three individual exposures were taken in order to correct for cosmic hits. The read-out mode for the spectra was chosen to be slow with a binning of 2×2 that lasted about 18 s. The data reduction procedure was performed using MIDAS. A routine procedure included trimming of the spectra, flat-fielding, bias subtraction and cosmic hit subtraction for which appropriate observations were made. The wavelength correction was provided using a spectrum of a He-Ar discharge lamp and flux calibration was done using a standard star (Hiltner 600). The obtained wavelengths were then again corrected for the barycentric radial velocity shift during exposure. The sky background was subtracted by extrapolating a sky-spectrum outside the region of interest. This data-set is extended with spectra recorded at 6″ and 11″ and is available from Van Winckel et al. (2002).

2.1. Astronomical results

Figure 1 presents an overview of the observational results. In all spectra the ERE is subtracted and spectra are stacked with an arbitrary offset, in order to allow for a better comparison. The emission features of the Na DII and DI lines at 5890 Å and 5896 Å are clearly visible in all spectra, as well as the Hα line at 6563 Å. The spectra furthermore show a number of other emission features; stronger ones around 5800–5900 Å that have been topic of several previous studies (Scarrott et al. 1992; Sarre et al. 1995) and many weaker features, up to 6800 Å. These spectra will be described in detail elsewhere (Wehres et al., in prep.). Here, we draw the attention to the clear spectral variations with distance to the star; new bands arise, some bands become more intense, whereas others clearly decrease in intensity. Overall the emission features seem to be quite sensitive to the change in environmental conditions in the Red Rectangle nebula. In our spectra we can see that the most prominent emission features between 5800 and 5900 Å show up already at 3″, whereas most

Table 1. NTT-EMMI telescope settings.

Distance to HD 44179 (arcsec)	Grating	Central wavelength (Å)	Wavelength coverage (Å)	Resolution $\lambda/\Delta\lambda$	Integration time (s)
0	6	5870	640	5000	60
0	6	6500	640	5000	60
3	6	5870	640	5000	500
3	6	6500	640	5000	500
7	6	5870	640	5000	2000
7	6	6500	640	5000	2000
16	7	6200	1300	2600	3600
20	7	6200	1300	2600	3600

Notes. The slit orientation is 105° east from north, perpendicular to the nebula's symmetry axis.

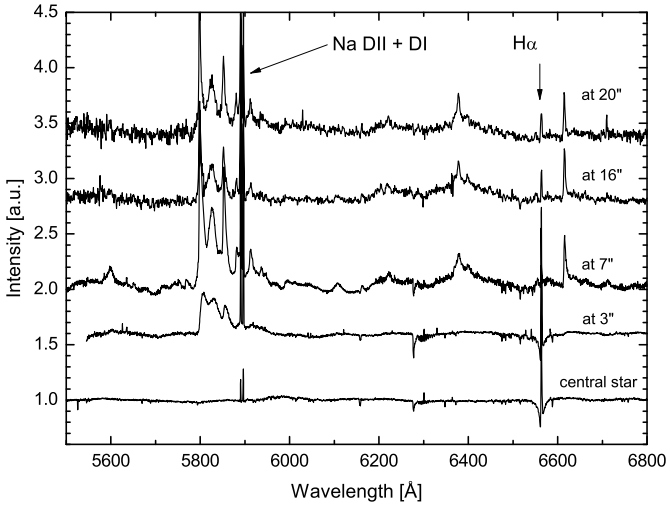

Fig. 1. Overview of all NTT-EMMI data taken towards HD 44179 on February 4 and 5, 2008. Complementary data for 6″ and 11″ (not shown) are available from Van Winckel et al. (2002).

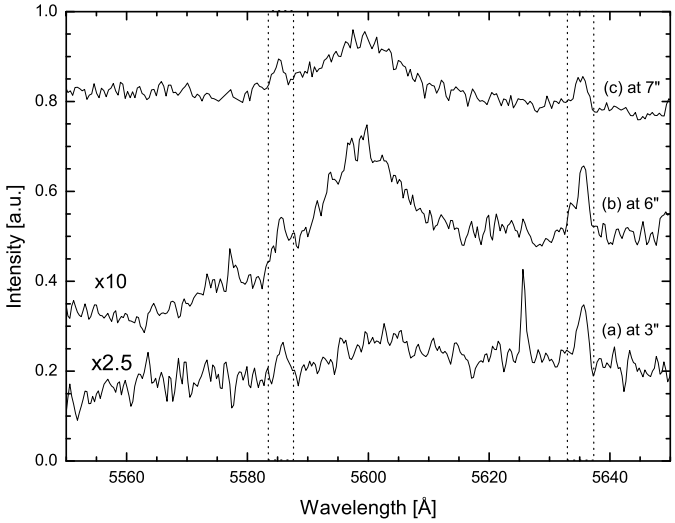

Fig. 2. Zoom-in on the Swan band $d^3\Pi_g \rightarrow a^3\Pi_u$ emission features at 3″, 6″ and 7″ offset from the central star.

of the other emission features become observable at larger distances from the star.

In this paper, we focus on two weak features in the 5550–5650 Å range of the observations at 3″, 6″ and 7″ distance from the central star (Fig. 2). Besides the broad and unidentified feature at 5600 Å, this zoom-in reveals two weaker bands at 5585 Å and 5635 Å that can be assigned to vibronic bands in the $d^3\Pi_g \rightarrow a^3\Pi_u$ $(v', v'') = (0, 1)$ and $(1, 2)$ Swan band system of C_2, as will be discussed. C_2 was identified in circumstellar material of post AGB stars (Bakker et al. 1996), in carbon rich outflows of proto-planetary nebulae (Klochkova et al. 1999), in cometary spectra (Gredel et al. 1989; Fink & Hicks 1996; Hobbs et al. 2004) and in interstellar clouds (Souza & Lutz 1977; Chaffee & Lutz 1978; Hobbs 1979; van Dishoeck & de Zeeuw 1984; Gredel 1999). In Sarre (2006) the C_2 (0,0) transition in the $d^3\Pi_g \rightarrow a^3\Pi_u$ at 5165 Å is mentioned for offsets up to 13″, but the corresponding spectrum was not shown. Very recently Glinski et al. (2009) showed a spectral overlap between a Red Rectangle emission band and a C_2 emission spectrum of the comet Hale-Bopp.

2.2. Laboratory experiment

An existing set-up (Volkers et al. 2004) designed for time-gated fluorescence spectroscopy of isotopologues of atmospheric interest (Volkers et al. 2006) has been modified by implementing a supersonic plasma source. This plasma source has been used previously to study vibrationally excited radicals at low rotational temperatures (Bazalgette Courrèges-Lacoste et al. 2001) and consists of a General Valve introducing a gas pulse in a multi-layer discharge geometry. Typically a 500 μs long negative high voltage discharge pulse (−700 V) is offered to a synchronized 700 μs long gas pulse of a 0.2% C_2H_2/He gas mixture that is expanded with a backing pressure of 4 bar into a vacuum chamber (10^{-5} mbar during jet operation) at a repetition rate of 10 Hz. The plasma expansion is intersected about 10 cm downstream by the output of a second harmonic Nd:YAG pumped tunable dye laser. The latter is operated on Rhodamine 6G dye and covers 5550 Å to 5850 Å. A single stage amplification scheme is used and maximum power ranges from 4 mW/pulse at 5650 Å to 0.5 mW/pulse at 5850 Å. The fluorescence signal is recorded by a photo-multiplier tube (PMT) using a time-gated integration scheme. The variable gate width of the PMT is necessary to prevent for saturation effects, because of light emission from the plasma source or by scattered laser light. Special care has been taken to reduce the amount of interfering light by also using light skimmers and band pass filters. The recorded spectra correspond to the intensity of the fluorescence signal at the PMT as a function of the incident photon wavelength. Calibration of the excitation wavelength is obtained by simultaneously recording an iodine absorption spectrum.

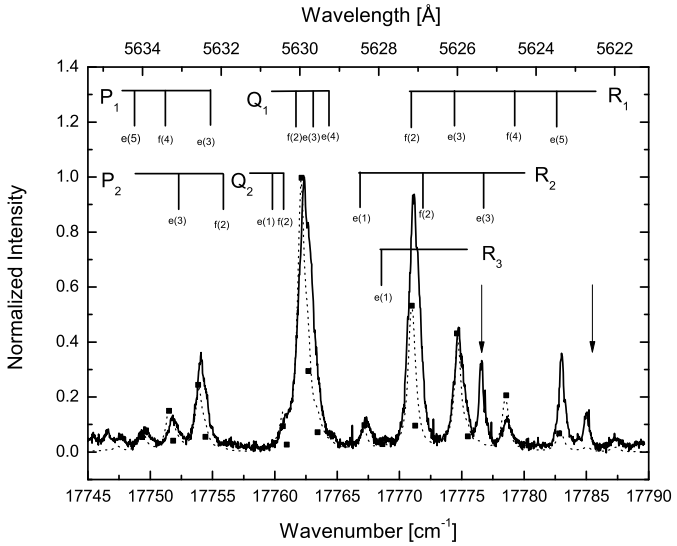

Fig. 3. A comparison of the experimental time gated and rotationally resolved fluorescence spectrum of the C_2 $d^3\Pi_g$ $v' = 0 \rightarrow a^3\Pi_u$ $v'' = 1$ Swan band transition (solid line) with a simulation calculated using the program PGOPHER (dotted line). The simulated spectrum has been arbitrarily normalized. Band assignments are shown at the top. The arrows indicate high temperature bands which are not modelled. See text for details.

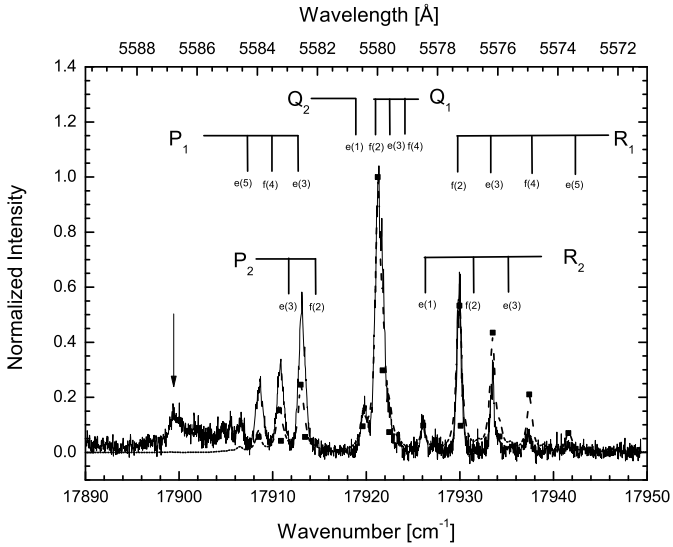

Fig. 4. A comparison of the experimental time gated and rotationally resolved fluorescence spectrum of the C_2 $d^3\Pi_g$ $v' = 1 \rightarrow a^3\Pi_u$ $v'' = 2$ Swan band transition (solid line) with a simulation calculated using the program PGOPHER (dotted line). The simulated spectrum has been arbitrarily normalized. Band assignments are shown at the top. The arrow indicates bandhead emission. See text for details.

2.3. Experimental results

Although we were expecting a rather congested spectrum, reflecting the many compounds that may be formed in the plasma expansion (Witkowicz et al. 2004) and likely present in the outflows of the Red Rectangle, we only recorded a limited set of rotationally resolved bands. In Figs. 3 and 4 two of these bands are shown in detail. These consist of a set of subsequent rovibronic transitions that can be assigned to Swan band transitions starting from the ground and vibrationally excited levels: $d^3\Pi_g$ $(v' = 0) \rightarrow a^3\Pi_u$ $(v'' = 1)$ and $d^3\Pi_g$ $(v' = 1) \rightarrow a^3\Pi_u$ $(v'' = 2)$. Due to the degeneracy of the triplet state, the rotational ladder splits into three separate, slightly staggered, sets of PQR rotationally resolved branches that reflect the substates (Curtis & Sarre 1985). Although C_2 is a very well studied molecule, high resolution laboratory emission studies are rare. Curtis & Sarre (1985) obtained high resolution C_2 spectra of the Swan band $(v = 0, 1)$ transitions using LIF spectroscopy with a mixture of Na and C_2Cl_4 reactants. Also Chen & Mazumder (1990) obtained emission spectra from a laser induced plasma during laser ablation of graphite in an Ar/He mixture. Their spectra are with a lower resolution. Most other studies comprise direct absorption spectroscopic techniques. As a consequence vibrationally excited levels are then only accessible in rather hot environments (i.e. discharge cells) with a number of disadvantages, such as spectral congestion and a lower detection sensitivity because of a lower state density. Comparable plasma sources have shown to generate a large sample of hydrocarbon radicals of the form $C_nH_m^{\pm}$ (Motylewski & Linnartz 1999; Witkowicz et al. 2004). In direct absorption rotational spectra of molecules like C_6H (Linnartz et al. 1999) or HC_6H^+ (Pfluger et al. 1999) have been observed. No evidence for fluorescence signals of such species has been found in the present experiment.

The two transitions reported in the laboratory spectra (Figs. 3 and 4) are the same transitions evident in the spectra of the Red Rectangle. The small shifts between observed and experimental spectra are due to different temperatures. We have simulated the spectrum of C_2 using the PGOPHER program (Western 2007) with standard molecular parameters as listed by Prasad & Bernath (1994) for the $a^3\Pi_u$ $v'' = 1$ and $v'' = 2$ levels and from Lloyd & Ewart (1999) and Prasad & Bernath (1994) for the $d^3\Pi_g$ $v' = 0$ and $v' = 1$ states. In Figs. 3 and 4, the experimental spectrum is plotted as a black solid line and shows the fluorescence intensity with respect to the excitation wavelength. Overplotted as a dotted line is a simulated spectrum. The linewidth of 0.65 cm^{-1} reflects residual Doppler broadening for an unskimmed beam expansion. The spectral pattern corresponds to a rotational temperature of about 15 K in the expansion. The plasma creates electronically and vibrationally hot molecules whereas the expansion adiabatically cools rotational motion. The result is vibrational excitation due to the discharge but low rotational temperatures due to subsequent cooling by carrier gas molecules.

The overall good agreement between experiments and calculations validates the use of the PGOPHER program to simulate the emission spectrum of C_2. There are small discrepancies between experiment and simulation. Specifically, at 5625 Å and 5623 Å the experimental spectrum shows two bands not reproduced by the simulations at 15 K (indicated with arrows; Fig. 3). Both bands do show up in the simulation at higher rotational temperatures. Also, Fig. 4 reveals a peak at 5587.0 Å (indicated with an arrow), that is not reproduced in the simulation and that corresponds to the bandhead. This indicates that not only a low temperature component is present in the expansion, but that also species are formed at substantially higher temperatures.

2.4. The C_2 rotational contour: excitation temperature and velocity shifts

The observed line profiles in the astronomical spectrum can in principal be used to estimate the rotational excitation temperature of C_2 in the Red Rectangle. Simulations, using PGOPHER (Western 2007) are compared to the observational spectra at 7″ in Fig. 5, assuming a single excitation temperature and

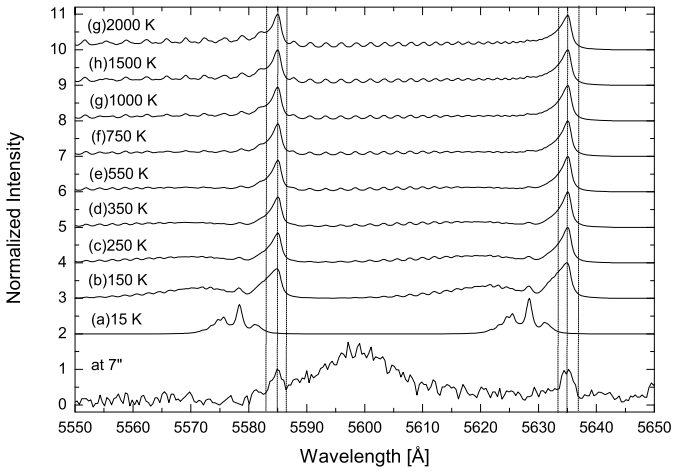

Fig. 5. Simulated line profiles of the Swan Band $d^3\Pi_g \rightarrow a^3\Pi_u$ emission features as a function of the rotational excitation temperature convolved to a resolution of 1.1 Å. These are compared to the observational spectrum at 7″. All spectra have been normalized and stacked with an arbitrary offset in order to allow for better comparison.

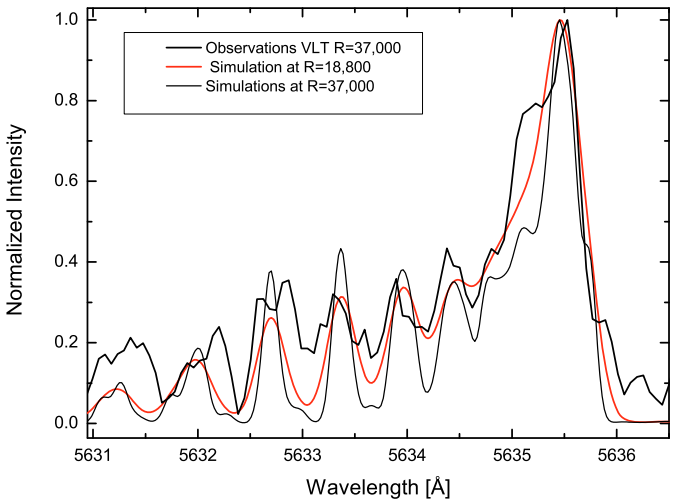

Fig. 6. VLT spectrum of the transition at 5635 Å (Glinski et al. 2009). The resolution of the observation is ~37 000. The observational spectrum is compared to simulations at a resolution of 37 000 and 18 800. The rotational temperature of the simulations is ~300 K.

convolved to the instrumental resolution of the observations (R = 5000). Both band profiles reveal a rotational temperature dependence. At low temperatures (<100 K), the PQR rotational structure is obvious, even when convolved to the low resolution of the observational data. As the temperature increases, the P-branch gains in intensity whereas the R-branch flattens. With the appearance of a more intense bandhead, the overall position also shows a shift to the red. This redshift is typical for molecules with a larger rotational constant in the upper state (v') than in the lower state (v''); the rotational constant in the $d^3\Pi_g \rightarrow a^3\Pi_u$ transition at 5585 Å is ≃1.7 cm^{-1} in the v' = 1 and ≃1.6 cm^{-1} in the v'' = 2 state for the $d^3\Pi_g \rightarrow a^3\Pi_u$ transition at 5635 Å it is ≃1.7 cm^{-1} in the v' = 0 state and ≃1.6 cm^{-1} in the v'' = 1 state. The bandhead becomes dominant at temperatures of ~150 K and develops a steep red edge. Starting with this temperature, the peak position of the unresolved bandhead also does not shift any further to the red. Only the line width shows then a slight temperature dependence, mainly due to increasing blending of the bandhead with R-band transitions (Fig. 5). It should be noted that for the same number of C_2 molecules, the bandhead intensity at 2000 K will be substantially lower than for 200 K. However, as this number is not known, we continue to work with normalized spectra and the resulting band width is used to obtain additional information. The fairly symmetric C_2 bands in the astronomical spectra and their peak positions (5635 and 5585 Å) reveal that the rotational temperature has to exceed ≃200 K and cannot be higher than ≃1000 K (Fig. 5).

A more recent spectrum of C_2 (Glinski et al. 2009) was obtained at substantially higher spectral resolution (R ≃ 37 000) and barely resolves the bandhead as well. In Fig. 6 we show the observational VLT spectrum overplotted by simulations for a rotational temperature of 300 K for two different resolutions. The simulation of this VLT data has to focus on the blended bandhead emission and this does not provide better constraints on the temperature of the emitting C_2 molecules. It does constrain however the velocity of the gas; e.g., in order to obtain a decent match on the steep red-edge of the bandhead, the observational spectrum had to be shifted about 0.025 nm ± 0.005 nm to the blue. Also, the simulated width of the bandhead emission is somewhat less than observed (Fig. 6). Convolving the simulated profile with a Gaussian with a Doppler broadening parameter of 5.8 km s^{-1} provides a good fit to the observations. The measured wavelength shift corresponds to a velocity of 13.3 km s^{-1} ± 3.7 km s^{-1}. We note that better constraints – particularly on the temperature – would be possible with a somewhat higher spectral resolution and a higher S/N observation that would resolve the individual R-branch transitions.

The observed C_2 bandhead shift is somewhat less than the systemic velocity shift of the gas as probed by various optical emission lines (18–19 km s^{-1}) (Van Winckel et al. 1995; Hobbs et al. 2004; Witt et al. 2009). The derived Doppler broadening parameter corresponds to a *FWHM* of an unblended rotational line of ≃14 km s^{-1}. This width is comparable to the narrow component, prominent in the Hα profile and the atomic (e.g., KI, CaII) and molecular lines (e.g., CH, CH^+, and CN) lines (Hobbs et al. 2004; Witt et al. 2009). Some atomic lines show a more complex velocity profile with two components, at 13 and 25 km s^{-1} (Sitko et al. 2008). Generally these components have comparable strength but not so for the Na D lines. A very broad Hα component as well as the fluorescent CO line emission in the UV reveal the presence of a hot (T ≃ 5500 K) fast molecular outflow (≃300 km s^{-1}). There is also evidence for a rotationally cold (T ≃ 50 K) but vibrationally excited CO component (T ≃ 2000 K) which requires no velocity shift and has a width of some 20 km s^{-1}, comparable to the value derived from the C_2 lines (Sitko et al. 2008). In contrast, the observed broadening of the C_2 bandhead is much larger than the width of the submillimeter, pure rotational, CO lines (≃5 km s^{-1}). Finally, the Hα and Na DI lines (as well as some of the UV lines of CO and OH) in the nebula are more highly polarized than the (ERE) continuum, indicating that they have a large or even dominant scattering contribution (Reese & Sitko 1996) and they may actually originate in the inner PDR zone that separates the ionized gas from the molecular torus. The Red Rectangle has been studied in depth in atomic and molecular lines as well as in the visible and infrared continuum emission (Witt et al. 2009; Waelkens et al. 1996; Bujarrabal et al. 2003, 2005; Hobbs et al. 2004; Cohen et al. 2004; Waters et al. 1998).

In view of the width, the C_2 emission may also originate in the PDR zone and not in the rotating, molecular disk. However, the small blue shift of the bandhead (relative to the atomic lines) indicates that the C_2 emission in the lobes has a slightly different

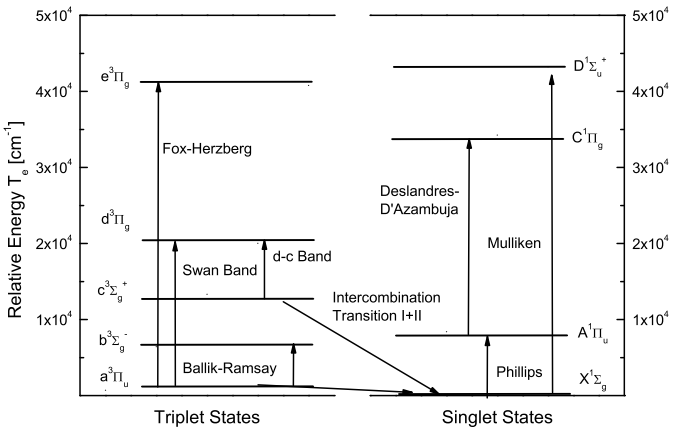

Fig. 7. An overview of the electronic energy states in C_2, summarizing the energy levels in C_2 and the corresponding energetics. Arrows indicate the most common transitions in the singlet and triplet system. The two arrows connecting the singlet and triplet states are schematics for "intercombination transitions", which are relevant in the excitation of C_2 because levels of the vibrational states in the $X^1\Sigma$ state and the $a^3\Pi$ state are close in energy.

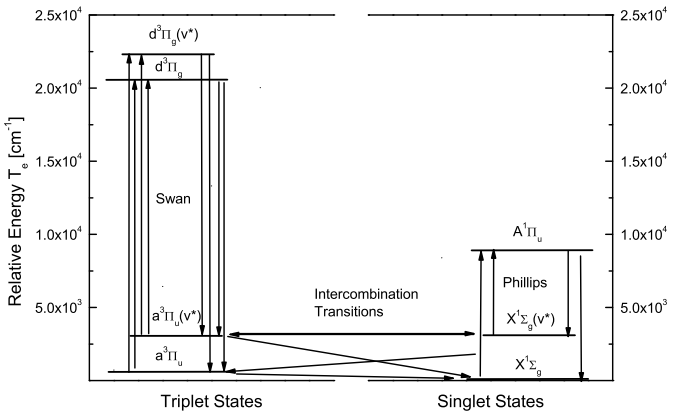

Fig. 8. Relevant energy levels of C_2 in the environment of the Red Rectangle nebula. Also shown schematically are the fiducial excited vibrational levels within these electronic states.

origin than these lines, and perhaps this molecular emission is due to material (partially) entrained in the jet while the atomic lines originate (by scattering) of the cavity walls.

3. Fluorescent emission in the Red Rectangle

3.1. Model

Now it is possible to combine these data to study the physical and chemical processes that are involved in the excitation mechanisms. For that reason, we present a model that accounts for the observed C_2 emissions in the Red Rectangle and that is also suited to infer quantitative information. Similar to comets, we attribute the Swan bands to fluorescent emission from C_2 pumped by stellar photons. In this model, the stellar wind from the central region is carbon-rich. Hence, all the oxygen is locked up in CO while the excess carbon is assumed to be in the form of C_2H_2. The acetylene is slowly photodissociated by UV photons from the star and/or from the putative accretion disk around the binary (Men'shchikov et al. 2002; Witt et al. 2009) to form sequentially C_2H, C_2, and eventually C. As we observe the C_2 signatures already at 3″ and they extend out to 13″ (Sarre 2006), this process has to start very quickly and be maintained for a long time compared to the outflow time scale (see also below). At any point, we will treat the C_2 abundance as in steady state between photoformation from a reservoir of C_2H_2 and photodestruction.

Following Gredel et al. (1989), we have examined all possible electronic transitions of C_2 up to the Mulliken band ~44 000 cm^{-1} (Fig. 7). Besides the regular radiative transitions, this also includes "intercombination transitions" between the singlet $X^1\Sigma_g^+$ and triplet $a^3\Pi_u$ levels. This analysis allows us to identify the energy levels that are important in view of the energy distribution of the Red Rectangle nebula (Fig. 8). Given the relatively low energy flux, especially in the UV in the Red Rectangle (Men'shchikov et al. 2002), the main pump from the singlet states to the triplet states is through the Phillips bands. Radiative excitation from the $X^1\Sigma_g^+$ to the $A^1\Pi_u$ state is rapidly followed by fluorescence which can leave the molecule in a vibrationally excited state of the ground electronic state, in the following defined as $X^1\Sigma_g^+(v^*)$. Because these states are close in energy to levels in the $a^3\Pi_u$ state, intercombination band transitions are rapid (van Dishoeck & Black 1982). The intercombination band from the lowest vibrational state of the $a^3\Pi_u$ state to the ground vibrational state of the $X^1\Sigma_g^+$ state is actually relatively slow and this transition presents a bottleneck in the "flow" (Le Bourlot & Roueff 1986). Once population has been transferred into the $a^3\Pi_u$ state, stellar photons can excite the $d^3\Pi_g$ state ($a^3\Pi_u \rightarrow d^3\Pi_g$) and its vibrationally excited levels ($a^3\Pi_g \rightarrow d^3\Pi_g(v^*)$) from which the observed Swan bands become visible in fluorescence. Both, the lowest vibrational level of the $d^3\Pi_g$ state and the excited vibrational levels of the $d^3\Pi_g(v^*)$ state, show emission as can be seen in our observational and laboratory spectra. Swan band fluorescence that leads to a vibrational excited level of the $a^3\Pi_u$ state most likely leads via the intercombination transition back into the singlet system. Actually, Swan band emission that leads to the lowest vibrational state of the $a^3\Pi_u$ state can be pumped several times into the $d^3\Pi_g$ state before an intercombination transition transfers the population back into the singlet state. How often the Swan band can be pumped in this way, before relaxing into the $X^1\Sigma_g^+$ state, is strongly dependent on the distance to the exciting star. Since the excitation of the vibrational levels in the ground state occurs via the Phillips band, pumped by stellar photons, the rate is inversely proportional to the distance squared. Intercombination transitions occur radiationless and are not dependent on the stellar flux. The pump in the triplet state is again dependent on the photon flux of the star and hence also scales inversely with the distance to the star squared. Overall, Swan band fluorescence scales in this excitation scheme, thus, inversely with distance to the fourth power.

Sophisticated models have been developed to determine the level populations of all rotational, vibrational, and electronic states involved in connection to the Swan band excitation in comets. However, the few levels observed in the Red Rectangle, the low resolution and relatively poor quality of the observed transitions does not warrant such an extensive model. Rather, we have developed a straight forward model which does retain, though, the essential aspects of the energy level diagram and the various pumps involved (Figs. 7 and 8). With respect to the stellar radiation field we include four electronic energy levels which are relevant for the pump scheme in the Red Rectangle (Fig. 8) – the singlet states, $X^1\Sigma_g^+$ and $A^1\Pi_u$, and the triplet states, $a^3\Pi_u$ and $d^3\Pi_g$ – and in order to mimic the intercombination and fluorescence transitions, we introduce three fiducial vibrational levels

Table 2. Rate coefficients for C_2 in the Red Rectangle at a distance of 6″ to the central star.

Number	Spontaneous emission	Rate[a] k [s^{-1}]	Number	Pumping transition	Rate[a] k [s^{-1}]	Number	Intercombination transition	Rate[a] k [s^{-1}]
1	$A^1\Pi_u \rightarrow X^1\Sigma_g^+$	5.1(4)	7	$X^1\Sigma_g^+ \rightarrow A^1\Pi_u$	4.0(−4)	13	$a^3\,\Pi_u \rightarrow X^1\Sigma_g^+$	3.8(−4)
2	$A^1\Pi_u \rightarrow X^1\Sigma_g^+(v^*)$	2.0(4)	8	$X^1\Sigma_g^+(v^*) \rightarrow A^1\Pi_u$	1.9(−4)	14	$a^3\Pi_u(v^*) \rightarrow X^1\Sigma_g^+(v^*)$	1.3(−2)
3	$d^3\Pi_g \rightarrow a^3\Pi_u$	7.0(6)	9	$a^3\Pi_u \rightarrow d^3\Pi_g$	1.7(−3)	15	$X^1\Sigma_g^+(v^*) \rightarrow a^3\Pi_u$	7.0(−2)
4	$d^3\Pi_g \rightarrow a^3\Pi_u(v^*)$	2.3(6)	10	$a^3\Pi_u(v^*) \rightarrow d^3\Pi_g$	7.1(−4)	16	$X^1\Sigma_g^+(v^*) \rightarrow a^3\Pi_u(v^*)$	5.5(−3)
5	$d^3\Pi_g(v^*) \rightarrow a^3\Pi_u$	2.8(6)	11	$a^3\Pi_u \rightarrow d^3\Pi_g(v^*)$	5.4(−4)	17	$a^3\Pi_u(v^*) \rightarrow X^1\Sigma_g^+$	1.0(−1)
6	$d^3\Pi_g(v^*) \rightarrow a^3\Pi_u(v^*)$	7.8(6)	12	$a^3\Pi_u(v^*) \rightarrow d^3\Pi_g(v^*)$	1.3(−3)			

Notes. [(a)] Values in brackets give exponents to base 10.

representing excited states, the $X^1\Sigma_g^+(v^*)$, $a^3\Pi_u(v^*)$ and $d^3\Pi_g(v^*)$. Rotational levels are not taken into account.

Einstein A coefficients for spontaneous emission have been obtained for a series of transitions using the calculated oscillator strengths by Kokkin et al. (2007). The results for the Phillips and the Swan bands agree well with the coefficients calculated by van Dishoeck (1983) and Gredel et al. (1989). From these we have determined representative transition rates (K_i) for the relevant ground and fiducial vibrational states (Table 2). The rates for the intercombination transitions between the singlet and triplet states were calculated using the transition dipole moments given by Gredel et al. (1989).

The results (Table 2) agree reasonably well with the outcome of the more detailed study by Le Bourlot & Roueff (1986) who provide intercombination transition rates split out to individual ro-vibrational levels. Einstein B coefficients for these transitions are calculated from the usual formulae linking the Einstein coefficients. Radiative excitation rates follow then by convolving these with the stellar spectrum for distances at 6″ (Table 2). We adopted a Kurucz $T_{\rm eff}$ = 7750 K, $\log g$ = 1.5 model for the visual spectrum normalized to a luminosity of 6050 $L_\odot$ (Men'shchikov et al. 2002). In our evaluation of the radiative pumping rates, we ignore extinction within the nebula and hence these rates scale simply inversely with the distance to the star squared. We have checked that stimulated emission can be ignored at these wavelengths. Special care was taken to ensure that transitions involving the fiducial vibrational levels have representative rates, where we realize that given the Einstein coefficients involved and the (likely) low optical depth in the pumping transitions, only the lowest vibrational levels have to be taken into account.

Here excitation of the relevant triplet states is mainly assumed to result from optical pumping of the singlet states followed by intersystem crossing. Other mechanisms, such as collisional pumping through H/H_2 collisions, electron impact excitation, or a non-thermal distribution following chemical reactions are considered to be less important. Given the low temperature and density of the gas, collisional excitation and de-excitation of the vibrational and electronic levels can be neglected as can be shown when adopting a hydrogen density as deduced from Men'shchikov et al. (2002) of $\sim 2.3 \times 10^4$ cm^{-3} for a distance of 6″. We assume a cross–section of C_2 given by $\sigma \sim 5 \times 10^{-16}$ cm^2 (van Dishoeck & Black 1982; Pouilly et al. 1983). Collisions will then occur with a rate of $\sim 2 \times 10^{-6}$ s^{-1}. This result is very small compared to spontaneous emission in either the singlet or the triplet excited electronic transitions (Table 2). The temperature in the outflow is low (200–1000 K) relative to the excitation energy of the relevant pumping levels (~10 000–25 000 K) and hence collisional pumping of either the Phillips or the Swan band transitions is negligible. Electrons in the outflow will be provided by ionization of carbon and their abundance will be small.

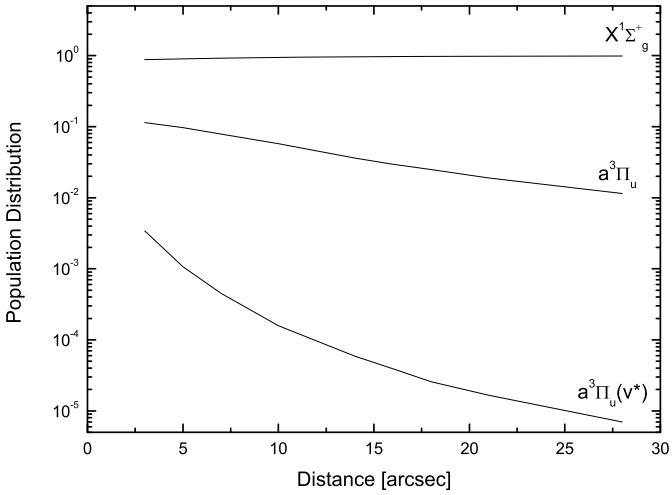

Fig. 9. Level populations in our fiducial C_2 molecule as a function of distance from the exciting star.

So, although their velocity is intrinsically much larger than for H atoms, electrons are also not important for excitation or de-excitation of the levels involved.

3.2. Results

The seven relevant energy levels in our fiducial C_2 model system are coupled by the radiative transitions illustrated in Fig. 8 with the rates given in Table 2. We solved the statistical equilibrium equations connecting these levels, combined with the abundance equation, and the results are given in Fig. 9 as a function of distance from the exciting star. Most of the C_2 molecules are in the ground state of the singlet system ($X^1\Sigma_g^+$). Appreciable population is transferred to the $a^3\Pi_u$ state, but its excitation is lower by one to two orders of magnitude depending on the distance to the exciting star. The population of the $a^3\Pi_u(v^*)$ state is down again by another one to two orders of magnitude at 6″. This just reflects the relatively slow pump in the Phillips band ($X^1\Sigma_g^+ \rightarrow A^1\Pi_u$) followed by the intercombination to the triplet state – that initiates the scheme – as compared to the intercombination transition channeling the triplet excitation back to the singlet state. Perusal of the rates in Table 2 shows that about 2/7 of the population in the $A^1\Pi_u$ is transfered into the excited fiducial level of the $X^1\Sigma_g^+(v^*)$ state, whereas the rest is transferred back into the ground state $X^1\Sigma_g^+$ (v = 0). Since C_2 is a homonuclear diatomic vibrational or rotational radiative relaxation from the exited fiducial level in the $X^1\Sigma_g^+$ to the ground level of the same electronic state is forbidden and hence intercombination

Table 3. Observed fluorescent intensities at 6″[a].

	Transition at 5585 Å	Transition at 5635 Å	Unit
Intensity	2.8 (−7) ± 0.6 (−7)	5.7 (−7) ± 0.6 (−7)	[erg cm^{-2} s^{-1} sr^{-1}]
Column density of fluorescing molecules in the (excited) d$^3\Pi_g$ state	4.0 (−1) ± 0.8 (−1)	1.0 ± 0.1	[cm^{-2}]
N(C$_2$)	1.1 (11) ± 0.2 (11)	6.3 (10) ± 0.6 (10)	[cm^{-2}]
C$_2$ abundance	5.7 (−11) ± 1.1 (−11)	3.9 (−11) ± 0.4 (−11)	

Notes. [(a)] Values in brackets give exponents to base 10.

transitions from the fiducial level of the $X^1\Sigma_g^+(v^*)$ state are effective in populating the $a^3\Pi_u$ state. The intercombination transition is also more efficient in transfering the population into the triplet system as excitation into another electronic level of the same multiplicity can take place. Eventually all population that reaches the fiducial level ($X^1\Sigma_g^+(v^*)$) is transferred into the triplet system.

Transitions back into the singlet state are slow and compete with excitation via stellar photons into the $d^3\Pi_g$ state (Table 2). The timescales for both transitions, the intercombination transition back into the ground state and the pump into the $d^3\Pi_g$ state are of the same order of magnitude at 6″ offset. The fast spontaneous emission in the Swan bands $d^3\Pi_g \rightarrow a^3\Pi_u$ keeps the population very low in the $d^3\Pi_g$ state as compared to the $X^1\Sigma_g^+$ and $a^3\Pi_u$. For distances (r), as close as 3″ to the exciting star, the pump rate into the $d^3\Pi_g$ state is about one order of magnitude higher compared to the intercombination transition back into the ground state. The population in the $a^3\Pi_g$ state is approximately given by,

$$\frac{n(a^3\Pi_u)}{n\,(X^1\Sigma_g^+)} = \frac{(\frac{k_2}{k_1+k_2})k_7}{(\frac{k_3}{k_3+k_4})k_9 + k_{13}} \quad (1)$$

$$\simeq 6.7\times10^{-2}\left(\frac{6''}{r''}\right)^2 \quad (2)$$

where the rates are given in Table 2. The population in the d$^3\Pi_g$ state per C$_2$ molecule can then be expressed, taking into account that nearly all C$_2$ molecules are in the $X^1\Sigma_g^+$ ground state; as follows:

$$\frac{n(\mathrm{d}^3\Pi_\mathrm{g})}{n(\mathrm{C}_2)} = \frac{k_9}{k_3}\,\frac{n(\mathrm{a}^3\Pi_\mathrm{u})}{n(\mathrm{C}_2)} \quad (3)$$

$$\simeq \frac{k_9}{k_3}\,\frac{(\frac{k_2}{k_1+k_2})k_7}{(\frac{k_3}{k_3+k_4})k_9 + k_{13}} \quad (4)$$

$$\simeq 1.6\times10^{-11}\left(\frac{6''}{r''}\right)^4. \quad (5)$$

The population in the $d^3\Pi_g$ state scales thus with the fourth power, since k$_9$ also scales inversely with distance squared. The last equation breaks down near the star when all of the C$_2$ is rapidly transferred into the triplet state ($n(\mathrm{a}^3\Pi_\mathrm{u}) \simeq n(\mathrm{C}_2)$). Similarly, for the excited state d$^3\Pi_g$ (v^*), we have

$$\frac{n(\mathrm{d}^3\Pi_\mathrm{g}\,(\mathrm{v}^*))}{n(\mathrm{C}_2)} = 3.5\times10^{-12}\left(\frac{6''}{r''}\right)^4. \quad (6)$$

3.3. The abundance of C_2

The average surface brightness in the observed Swan band transitions corrected for the ERE is provided in Table 3. These observed intensities can be directly translated into the number of fluorescing molecules in the relevant d$^3\Pi_g$ states using the Einstein A coefficients of both transitions (~2.52×10^6 s^{-1} for the $(v', v'') = (1, 2)$ at 5585 Å; ~1.95×10^6 s^{-1} for the $(v', v'') = (0, 1)$ at 5635 Å). We have used our fiducial model to translate these into the column density of C$_2$ molecules present at 6″ distance from the star in the Red Rectangle (Eqs. (3) and (6)). The two transitions yield values for the total C$_2$ column density at this distance within 25%, surely coincidental, given the approximate nature of our model.

The abundance of C$_2$ in the Red Rectangle is calculated adopting the simple model for the Red Rectangle developed to explain the IR continuum emission (Men'shchikov et al. 2002). In this model, the cone has a number density of ~5×10^5 molecules cm^{-3} at $r_o = 2.8''$ with a steep density gradient in the outer extended envelope of the nebula of $\rho \sim r^{-4}$. This yields a hydrogen density of 2.4×10^3 cm^{-3} at 6″. Assuming circular symmetry for the outflow cone, the total hydrogen column density is 2×10^{21} cm^{-2}. The C$_2$ abundance is then ~5×10^{-11} (Table 3). Note that this analysis assumes that the bandhead emission contains most of the emission. As Fig. 5 demonstrates this is reasonable for temperatures between 200 K and 1000 K. In addition, this abundance determination assumes the density distribution of Men'shchikov et al. (2002) and the uncertainty associated with this assumption is difficult to estimate.

4. Implications

We have derived a total C$_2$ abundance of ~5×10^{-11} at a distance of 6″ to the central star (Table 3). For comparison, typical column densities and abundances of C$_2$ in diffuse clouds are 3×10^{13} cm^{-2} and ~10^{-8}, respectively, as measured through absorption in the Phillips bands. However, in this comparison it should be noted that absorption line studies are done along a pencil beam against a stellar continuum source ($R_* \simeq 30\,R_\odot$) and hence the total number of C$_2$ molecules "observed" is ~3×10^{38}. In contrast, the total number of C$_2$ molecules "observed" in the nebula of the Red Rectangle at 6″ is ~4×10^{44}. So, while only one out of every ~15 C$_2$ molecules is in the triplet system and only one out of every 10^{11} fluorescing photons is emitted into our beam, we are still sensitive enough to observe the fluorescence because there are six orders of magnitude more C$_2$ molecules in our slit than in the astronomical absorption experiment.

While the abundance of C$_2$ is low, this still provides some further insight in the origin of this species. With a UV photodissociation cross section of 0.5×10^{-17} cm^2 at 10.6 eV and 0.77×10^{-17} cm^2 at 12.2 eV (Pouilly et al. 1983), the photodissociation rate at 6″ of C$_2$ is ~4×10^{-7} s^{-1} if the UV light is dominated by the star (adopting the parameters of Men'shchikov et al. (2002) ($T_{\rm eff} = 7750$ K, $\log g = 1.5$) and ≃2×10^{-5} if the putative accretion disk (with $\dot{M}_{\rm acc} = 10^{-4}\,M_\odot$/yr; Witt et al. 2009) is responsible for the UV emission. Hence, irrespective of the origin of the dissociating UV photons, the lifetime of a

C_2 molecule is very short in the nebula (e.g., one day to one month). This is much shorter than the outflow timescale at this distance ($R/v \simeq 3000$ yr for an outflow velocity of 7 km s^{-1}) and hence, the C_2 has to be rapidly replenished. This cannot come from C_2H_2 or C_2H since the photodissociation rate of these species are some ten times faster than that of C_2 (Pouilly et al. 1983; van Hemert & van Dishoeck 2008; Nee & Lee 1984) . Assuming that the C_2 is derived from a major reservoir of the carbon such as PAHs, which contains 10% of the elemental carbon, the (photo)destruction rate of this reservoir has to be $\simeq 10^{-6}$ that of C_2, e.g., a dissociation timescale of 10^3–10^4 yr. Quite reasonable given the outflow timescale. Conversely, the parent species of C_2 (and by inference, C_2H_2) has to represent a major reservoir of the elemental carbon. We note that subtle variations in the profiles of the IR emission features with distance from the exciting star in the Red Rectangle have been interpreted in terms of chemical changes in the PAH family (Song et al. 2007). Quantitatively, adopting a UV absorption cross-section of 7×10^{-18} cm^2 (C-atom)$^{-1}$, we estimate an absorption rate of UV photons of $\simeq 4 \times 10^{-4}$ s^{-1} with $h\nu > 6$ eV and about $\simeq 10^{-5}$ s^{-1} with $h\nu > 10$ eV, for a 50 C-atom PAH at a distance of 6″ from the star. In order to explain the observed abundance of C_2, the photo-destruction probability of PAHs should then be 10^{-9} and 3×10^{-8}, respectively. This corresponds to the estimated photo-destruction rate of 10^{-6} compared to that of C_2. In a recent analysis of PAH destruction in the ISM, Micelotta et al. (2010) estimated a photo-destruction probability that is slightly higher (5×10^{-7}). Future laboratory experiments will be instrumental to determine whether such photo-destruction probabilities are realistic for large PAHs. Finally, we note that PAHs are not the only conceivable source of C_2H_2 parents for the observed C_2. Hydrogenated Amorphous Carbon grains, HACs, are also an important reservoir of carbon in the outflow of the Red Rectangle. Recent studies have suggested that cycling of carbon in and out of dust is an important source of small hydrocarbon species (Jones 2009; Pety et al. 2005). Besides photo-destruction, in this case, these grains may also be broken down by shocks. Weak, extended Hα emission indicates the importance of shocks in the outflow itself (Cohen et al. 2004). Grain-grain collisions in the shock may lead to fragmentation and molecule formation (Jones et al. 1996).

Finally, we note that the pumping rate in the Phillips and Swan bands – which is at the base of the fluorescence model – well exceeds the photo–destruction rate and therefore many Swan band photons are produced before C_2 is destroyed. Hence, excitation of the Swan band system at formation is an ineffective pump relative to the visible fluorescence. The more since only 5% of C_2 resulting from photo-dissociation of C_2H is formed in the triplet state (Sorkhabi et al. 1997; Wodtke & Lee 1985).

5. Conclusions

1. The Swan band transitions of $d^3\Pi_g \rightarrow a^3\Pi_u$ type $(v', v'') = (0, 1)$ and $(v', v'') = (1, 2)$ type have unambiguously been identified in the outflow of the Red Rectangle protoplanetary nebula. We have simulated the spectra using the rotational contour program PGOPHER. The simulation was validated against a laboratory study of C_2 obtained in a supersonic plasma expansion. These simulations constrain the rotational temperature of C_2 in the Red Rectangle to be not lower than 200 K and not higher than 1000 K.
2. The mechanism for excitation and de-excitation has been established within the conditions of the Red Rectangle nebula. Our modelling of the excitation and de-excitation mechanism shows that the excitation of the C_2 molecule in that environment is most likely due to transitions leading from the $X^1\Sigma_g^+$ ground state of the molecule via the Phillips Band to the $A^1\Pi_u$ state. From here the higher vibrational levels of the $X^1\Sigma_g^+$ can be efficiently populated and a population transfer from the singlet to the triplet state is possible ($X^1\Sigma_g^+ \rightarrow a^3\Pi_u$). Once this level is populated, the absorption into the $d^3\Pi_g$ state is followed very efficiently by spontaneous emission in the Swan band.
3. We have developed a model for the C_2 emission in the Red Rectangle. This model has been used to translate the observed strength of the Swan band transitions in the Red Rectangle into a local C_2 abundance. The results reveal that the C_2 abundance is very low $\sim 5 \times 10^{-11}$.
4. Visible fluorescence in a nebular setting is potentially a powerful probe of the presence of molecular species if suitable electronic states can be populated and depopulated through electronic transitions.
5. The inferred abundance of C_2 implies that C_2 derives from a major reservoir of the elemental carbon in the outflow which is slowly destroyed – likely first into C_2H_2 and then C_2 – on a timescale which is comparable to the outflow timescale of the nebula (3000 yr). Presumably, small PAH molecules represent this reservoir.
6. The experimental set-up shows the potential to simulate the physical conditions as constrained from observations and modelling in the Red Rectangle. In a discharge expansion molecules are created as observed in the emission bands from the Red Rectangle. Rotationally resolved spectra from vibronically excited species show potential for further comparison with the Red Rectangle emission features.

Acknowledgements. N.W. acknowledges the financial support provided through the European Communitys Human Potential Programme under contract, MCRTN 512302, Molecular Universe. This work was supported by the Netherlands Research School For Astronomy (Nederlandse Onderzoeksschool voor Astronomie) NOVA and the Sackler Laboratory for Astrophysics at Leiden University. We acknowledge R. Glinski for kindly making the VLT data available. We gratefully acknowledge fruitful discussion with E. van Dishoeck on the excitation of C_2.

References

Bakker, E. J., van Dishoeck, E. F., Waters, L. B. F. M., & Schoenmaker, T. 1996, VizieR Online Data Catalog, 332, 30469
Bazalgette Courrèges-Lacoste, G., Sprengers, J. P., Bulthuis, J., et al. 2001, Chem. Phys. Lett., 335, 209
Bond, H. E. 1997, in IAU Symp. 180, Planetary Nebulae, ed. H. J. Habing & H. J. G. L. M. Lamers, 460
Bujarrabal, V., Neri, R., Alcolea, J., & Kahane, C. 2003, A&A, 409, 573
Bujarrabal, V., Castro-Carrizo, A., Alcolea, J., & Neri, R. 2005, A&A, 441, 1031
Chaffee, Jr., F. H., & Lutz, B. L. 1978, ApJ, 221, L91
Chen, X., & Mazumder, J. 1990, Appl. Phys. Lett., 57, 2178
Cohen, M., Anderson, C. M., Cowley, A., et al. 1975, ApJ, 196, 179
Cohen, M., Van Winckel, H., Bond, H. E., & Gull, T. R. 2004, AJ, 127, 2362
Curtis, M. C., & Sarre, P. J. 1985, J. Mol. Spectrosc., 114, 427
Duley, W. W. 1985, MNRAS, 215, 259
Fink, U., & Hicks, M. D. 1996, ApJ, 459, 729
Glinski, R. J., & Anderson, C. M. 2002, MNRAS, 332, L17
Glinski, R. J., Michaels, P. D., Anderson, C. M., et al. 2009, Ap&SS, 145
Gredel, R. 1999, A&A, 351, 657
Gredel, R., van Dishoeck, E. F., & Black, J. H. 1989, ApJ, 338, 1047
Hall, K. I., Miles, J. R., Sarre, P. J., & Fossey, S. J. 1992, Nature, 358, 629
Hobbs, L. M. 1979, ApJ, 232, L175
Hobbs, L. M., Thorburn, J. A., Oka, T., et al. 2004, ApJ, 615, 947
Jones, A. P. 2009, The Cycle of Carbon Dust in the ISM: Cosmic Dust Near and Far Proceedings, ed. Th. Henning, E. Grn, & J. Steinacker, ASP, 414, 473
Jones, A. P., Tielens, A. G. G. M., & Hollenbach, D. J. 1996, ApJ, 469, 740
Jura, M., Turner, J., & Balm, S. P. 1997, ApJ, 474, 741

Klochkova, V. G., Szczerba, R., Panchuk, V. E., & Volk, K. 1999, A&A, 345, 905
Kokkin, D. L., Bacskay, G. B., & Schmidt, T. W. 2007, J. Chem. Phys., 126, 084302
Le Bourlot, J., & Roueff, E. 1986, J. Mol. Spectrosc., 120, 157
Ledoux, G., Ehbrecht, M., Guillois, O., et al. 1998, A&A, 333, L39
Ledoux, G., Guillois, O., Huisken, F., et al. 2001, A&A, 377, 707
Leger, A., & Puget, J. L. 1984, A&A, 137, L5
Linnartz, H. 2009, Cavity ring down spectroscopy of molecular transients of astrophysical Interest, Blackwell publishers; ed. G. Berden, & R. Engeln, 145
Linnartz, H., Motylewski, T., Vaizert, O., et al. 1999, J. Mol. Spectrosc., 197, 1
Linnartz, H., Wehres, N., van Winckel, H., et al. 2010, A&A, 511, L3+
Lloyd, G. M., & Ewart, P. 1999, J. Chem. Phys., 110, 385
Men'shchikov, A. B., Schertl, D., Tuthill, P. G., Weigelt, G., & Yungelson, L. R. 2002, A&A, 393, 867
Micelotta, E. R., Jones, A. P., & Tielens, A. G. G. M. 2010, A&A, 510, A37+
Motylewski, T., & Linnartz, H. 1999, Rev. Sci. Instr., 70, 1305
Nee, J., & Lee, L. 1984, JCP, 81, 31
Osterbart, R., Langer, N., & Weigelt, G. 1997, A&A, 325, 609
Pety, J., Teyssier, D., Fossé, D., et al. 2005, A&A, 435, 885
Pfluger, D., Sinclair, W. E., Linnartz, H., & Maier, J. P. 1999, Chem. Phys. Lett, 313, 171
Pouilly, B., Robbe, J. M., Schamps, J., & Roueff, E. 1983, J. Phys. B Atomic Molec. Phys., 16, 437
Prasad, C. V. V., & Bernath, P. F. 1994, ApJ, 426, 812
Reese, M. D., & Sitko, M. L. 1996, ApJ, 467, L105
Roddier, F., Roddier, C., Graves, J. E., & Northcott, M. J. 1995, ApJ, 443, 249
Russell, R. W., Soifer, B. T., & Willner, S. P. 1978, ApJ, 220, 568
Sarre, P. J. 2006, J. Mol. Spectrosc., 238, 1
Sarre, P. J., Miles, J. R., & Scarrott, S. M. 1995, Science, 269, 674
Scarrott, S. M., Watkin, S., Miles, J. R., & Sarre, P. J. 1992, MNRAS, 255, 11
Schmidt, G. D., Cohen, M., & Margon, B. 1980, ApJ, 239, L133
Sharp, R. G., Reilly, N. J., Kable, S. H., & Schmidt, T. W. 2006, ApJ, 639, 194
Sitko, M. L., Bernstein, L. S., & Glinski, R. J. 2008, ApJ, 680, 1426
Song, I., McCombie, J., Kerr, T. H., & Sarre, P. J. 2007, MNRAS, 380, 979
Sorkhabi, O., Blunt, V., Lin, H., et al. 1997, JCP, 107, 9842
Souza, S. P., & Lutz, B. L. 1977, BAAS, 9, 354
van Dishoeck, E. F. 1983, Chem. Phys., 77, 277
van Dishoeck, E. F., & Black, J. H. 1982, ApJ, 258, 533
van Dishoeck, E. F., & de Zeeuw, T. 1984, MNRAS, 206, 383
van Hemert, M. C., & van Dishoeck, E. F. 2008, Chem. Phys., 343, 292
Van Winckel, H., Waelkens, C., & Waters, L. B. F. M. 1995, A&A, 293, L25
Van Winckel, H., Cohen, M., & Gull, T. R. 2002, A&A, 390, 147
Vijh, U. P., Witt, A. N., & Gordon, K. D. 2004, ApJ, 606, L65
Vijh, U. P., Witt, A. N., & Gordon, K. D. 2005, ApJ, 619, 368
Vijh, U. P., Witt, A. N., York, D. G., et al. 2006, ApJ, 653, 1336
Volkers, E. A., Vredenborg, A., Linnartz, H., et al. 2004, Chem. Phys. Lett., 391, 106
Volkers, E. A., Bulthuis, J., Stolte, S., Jost, R., & Linnartz, H. 2006, J. Mol. Spectrosc., 237, 259
Waelkens, C., Van Winckel, H., Waters, L. B. F. M., & Bakker, E. J. 1996, A&A, 314, L17
Waters, L. B. F. M., Cami, J., de Jong, T., et al. 1998, Nature, 391, 868
Western, C. M. 2007, University of Bristol, http://pgopher.chm.bris.ac.uk
Witkowicz, E., Linnartz, H., de Lange, C., et al. 2004, Int. J. Mass Spec., 232, 25
Witt, A. N., & Boroson, T. A. 1990, ApJ, 355, 182
Witt, A. N., & Vijh, U. P. 2004, in Astrophysics of Dust, ed. A. N. Witt, G. C. Clayton, & B. T. Draine, ASP Conf. Ser., 309, 115
Witt, A. N., Gordon, K. D., & Furton, D. G. 1998, ApJ, 501, L111
Witt, A. N., Mandel, S., Sell, P. H., Dixon, T., & Vijh, U. P. 2008, ApJ, 679, 497
Witt, A. N., Vijh, U. P., Hobbs, L. M., et al. 2009, ApJ, 693, 1946
Wodtke, A., & Lee, Y. 1985, J. Phys. Chem., 89, 4744